ORGANIC CHEMISTRY FRONTIERS

RESEARCH ARTICLE

View Article Online
View Journal | View Issue

Cite this: *Org. Chem. Front.*, 2021, **8**, 1775

Design, synthesis, and properties of a six-membered oligofuran macrocycle†

Anthony J. Varni,[a] Manami Kawakami,[a] Stephanie A. Tristram-Nagle,[b] David Yaron,[a] Tomasz Kowalewski *[a] and Kevin J. T. Noonan *[a]

Received 8th October 2020,
Accepted 21st January 2021

DOI: 10.1039/d1qo00084e

rsc.li/frontiers-organic

Herein, we present the synthesis and properties of an ester-functionalized macrocyclic sexifuran (C6FE). This molecule was prepared in a single step from a furan-3-carboxylate dimer using a commercially available palladium catalyst (SPhos-Pd-G3) and isolated in 34% yield. DFT calculations predict the macrocyclic ring is planar, with minimal ring strain. The macrocycle is partially crystalline, as evidenced by powder X-ray diffraction patterns. Furthermore, the solid-state organization can be altered by modification of the ester side-chain. C6FE can also undergo two electron oxidation and reduction in solution as evidenced by cyclic voltammetry. Quantum chemical investigations revealed how aromaticity along the entire sexifuran macrocycle may play a role in the reversible electrochemistry. Overall, we anticipate that the synthetic approach detailed in this report can serve as a foundation to construct new furan-based conjugated macrocycles.

Introduction

Conjugated macrocycles are of interest as components in organic materials,[1–3] host–guest chemistry,[2,3] and supramolecular design.[2–8] The properties of these shape-persistent cyclic oligomers are dictated by the identity of the repeat unit, in addition to the size and shape of the overall structure. Herein, we present the optoelectronic and solid-state characterization of an ester-functionalized, six-membered macrocyclic oligofuran (cyclo[6]furan-3-ester or C6FE in Chart 1). To our knowledge, a macrocycle constructed purely from furan rings has only been reported once before.[9] C6FE is synthesized in a single step using Suzuki–Miyaura cross-coupling, capitalizing on a steric interaction which destabilizes the *anti* configuration and an H-bonding interaction that favours the *syn* configuration of adjacent repeat units.[10] Furthermore, quantum chemical calculations are used to gain additional insight into the electronic structure of C6FE and how global aromaticity[11–14] plays a role in redox-state stabilization.

Generally, the geometric features of conjugated macrocycles are dictated by the choice of repeat unit, oligomer size, and degree of strain. Benzenoids, for example, are quite versatile, as a wide range of molecular shapes (belts, loops and bowls) can be accessed.[15–17] Benzenoid macrocycles can also be converted to planar constructs when the arene is substituted at the 1 and 3 positions, and spacer groups (*e.g.* acetylene) are inserted between the 6-membered rings, but these lack significant conjugation due to the *meta* substitution pattern. Five-

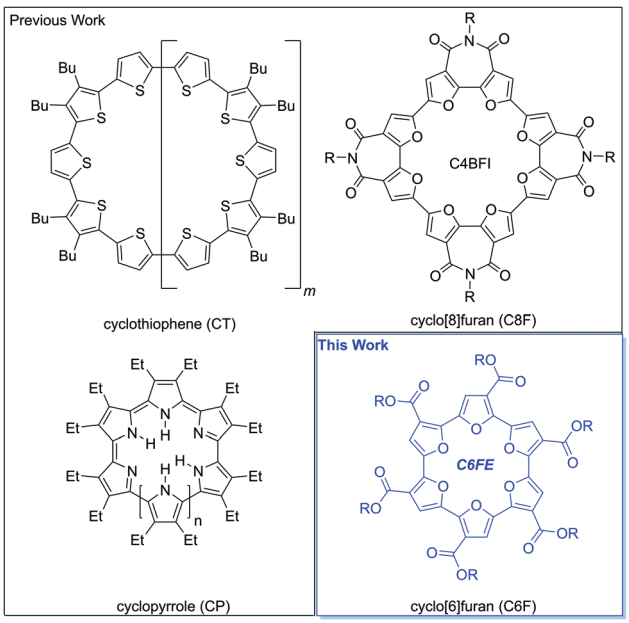

Chart 1 Families of macrocycles derived from heterocycles with no spacers. A series of CT macrocycles have been isolated (m = 1–6).[27] For CPs, n = 1–3. For C4BFI, the R group is a 2-octyldodecyl chain.

[a]*Department of Chemistry, Carnegie Mellon University, Pittsburgh, Pennsylvania 15213-2617, USA. E-mail: noonan@andrew.cmu.edu, tomek@andrew.cmu.edu*
[b]*Physics Department, Carnegie Mellon University, Pittsburgh, Pennsylvania 15213-2617, USA*

†Electronic supplementary information (ESI) available. See DOI: 10.1039/d1qo00084e

membered heterocycles provide unique geometric constraints relative to benzenoids, and a 2,5-substitution on the five-membered ring can be used to maintain strong conjugation between repeat units while still facilitating formation of a flat cyclic structure.

Cyclopyrroles are an important class of expanded porphyrins[18,19] with no methine spacers between heterocyclic repeat units (Chart 1). These have been synthesized with different numbers of pyrroles (n = 1–3),[20–22] they can be complexed with metals,[23] they have interesting electronic properties,[24] and the doubly protonated forms have been examined using magnetic circular dichroism.[25] For group 16 heterocycles, thiophenes have been explored extensively to build macrocycles (Chart 1),[26–35] but small rotational barriers about the interring bond can allow for distortions from planarity.[36] Furan repeat units, by contrast, strongly favor coplanar geometry,[37–46] and are much more reluctant to twist.[42,45] Computational work has suggested that furan building blocks can be used to create very compact, planar cyclic oligomers when compared to thiophenes.[47] Despite this potential, only a few reports have appeared on furan-containing macrocycles,[48–52] of which only a single report has appeared without spacer groups (cyclo-4-bifurandiimide or C4BFI).[9] Our results suggest that non-covalent interactions are a powerful tool to prepare CFs with minimal ring-strain.

Results and discussion

Synthesis

In prior work, we detailed the preparation of a helical poly(3-hexylesterfuran) (P3HEF shown in Fig. 1).[10] The electron-withdrawing ester side groups resulted in spontaneous adoption of a compact helical polymer conformation, driven by a 4.0 kcal mol^{-1} preference for *syn* coplanar orientation of adjacent ester-functionalized furan units. Based on the number of repeat units per turn (6.5 rings), we anticipated that the furan-ester subunit could also template the synthesis of six and/or seven membered macrocycles. DFT calculations supported this hypothesis, revealing low ring strains for both species (Fig. S1–S3†).

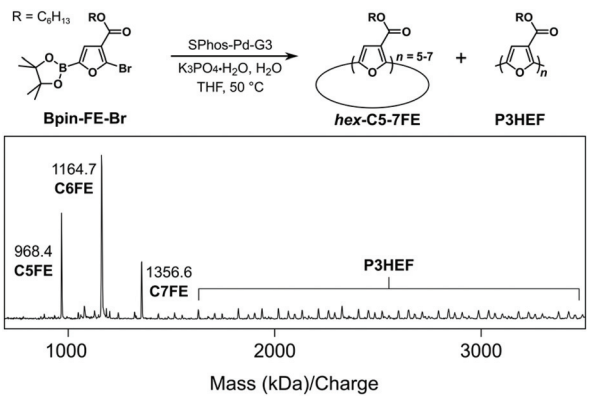

Fig. 1 Reaction conditions for one-step cyclization using Bpin-FE-Br and the possible products (top). MALDI-TOF spectrum of the crude product mixture when attempting the one-step macrocyclization with Bpin-FE-Br (bottom).

A commercially available palladium catalyst[53] (G3-Pd-SPhos) was employed in all macrocyclization experiments. The choice of catalyst for this reaction is critical to promote formation of the macrocycle, as the M(0) catalyst is needed to ensure no defects arise from the side group orientation. Reduction of metal dihalides for example, would produce a tail-to-tail orientation of esters,[54,55] and impact the conformational preferences of adjacent furans (Fig. S4†).

The combination of Bpin-FE-Br with G3-Pd-SPhos produced a mixture of cyclic oligofurans, since ring-closing can occur whenever oligomer ends are in proximity (C5FE up to C7FE, Fig. 1). DFT calculations did indeed suggest that the uncyclized 5FE, 6FE, and 7FE satisfy this condition (Fig. S1†), and that cyclized C6FE and C7FE have lower ring strain than C5FE (Fig. S3†). To facilitate preferential formation of macrocycles containing the same even number of repeat units, a "dimer" monomer was synthesized (Bpin-FEFE-Br, Fig. 2a). Only the hexameric macrocycle (*hex*-C6FE) was formed upon cross-coupling of Bpin-FEFE-Br with SPhos-Pd, in addition to polymeric byproduct (P3HEF), as evidenced by MALDI-TOF mass spectrometry (Fig. 2a). This ring is predicted to be perfectly planar with a 5.11 Å cavity as determined using DFT calculations (Fig. 2b). The *hex*-C6FE macrocycle was isolated using column chromatography, in reasonable yield (34%) when compared to other conjugated macrocycle syntheses.[2,56]

A single sharp aromatic resonance is observed in the ^{1}H NMR spectrum of *hex*-C6FE, as expected for the 6 equivalent furan rings (7.50 ppm, H_A, Fig. 2c). The diagnostic methylene protons of the hexyl ester side chain appear as a triplet at 4.19 ppm ($^3J_{HH}$ = 7.2 Hz, H_B, Fig. 2c). The well-defined spectrum of *hex*-C6FE is in stark contrast to the ^{1}H NMR signals of our previously reported helical polyfuran,[10] which are remarkably broad due to the structure's rigidity (resulting in inequivalent chemical environments) and slow tumbling in solution. The ^{13}C NMR spectrum of *hex*-C6FE also supports the macrocycle assignment (Fig. 2d) with eleven total signals for the oligomer (four aromatic, six aliphatic, and one carbonyl). The signals at 149.1 ppm and 144.2 ppm correspond to the carbon atoms adjacent to the furan oxygen (C2/C5), and the near overlapping signals at 116.4 ppm and 116.3 ppm correspond to the C3/C4 positions.

Optical properties and aggregation in solution

Hex-C6FE absorbs mostly in the UV region, with a λ_{max} at 352 nm ($\varepsilon = 1.3 \times 10^5$ cm^{-1} M^{-1}) (solid black trace in Fig. 3a). This is in general agreement with the TD-DFT prediction of an intense $S_0 \rightarrow S_2/S_3$ transition (dotted black trace in Fig. 3a). The HOMO and LUMO orbitals have identical symmetry (Fig. 3a), and therefore the $S_0 \rightarrow S_1$ transition is forbidden according to Laporte's rule. The presence of distinct bands in the spectrum is likely caused by an interplay between the intrinsic vibronic structure expected in a rigid macrocycle, and some intermolecular aggregation. Change of the overall sym-

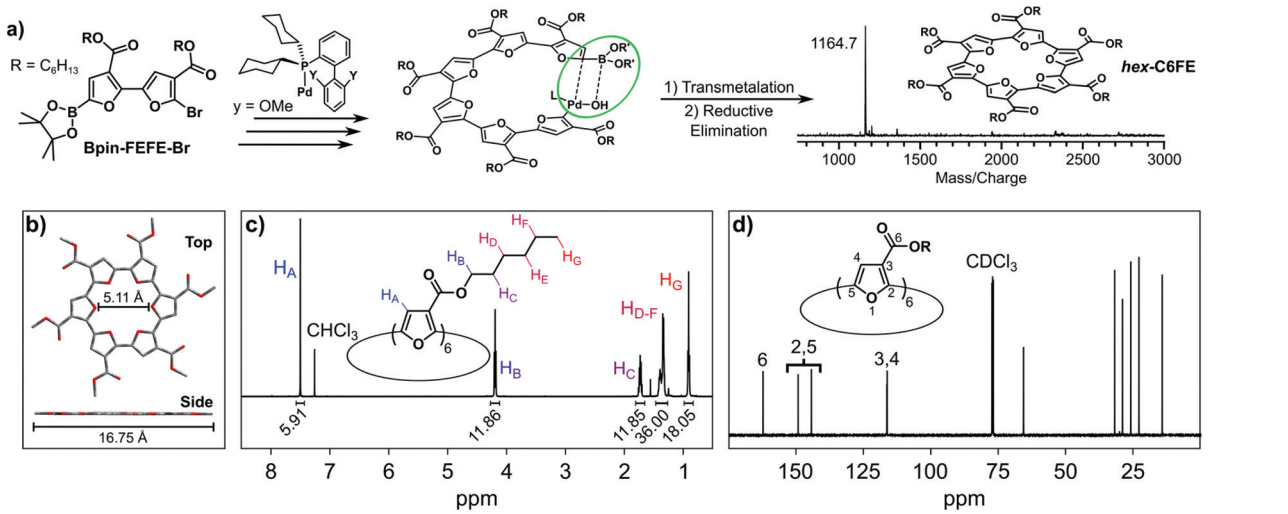

Fig. 2 (a) One-step synthesis of *hex*-C6FE from the "dimer-type" monomer (Bpin-FEFE-Br) using a palladium dialkylbiarylphosphine catalyst (SPhos-Pd), with MALDI-TOF of the crude product (right). (b) Structure of *me*-C6FE optimized using DFT (B3LYP-D3 6-31G(d,p)). In all computational work, alkyl chains were replaced with methyl groups to decrease computational time. (c) ^{1}H NMR (500 MHz) and (d) ^{13}C NMR (126 MHz) spectra of *hex*-C6FE acquired at 22 °C in $CDCl_3$.

metry due to aggregation can be also invoked to explain the presence of a weak band near the expected HOMO–LUMO transition (~500 nm).

Self-association of molecules containing aromatic moieties can be quantified by ^{1}H NMR, by fitting the characteristic upfield shift of aromatic protons due to additional shielding.[57–59] Analysis of the series of spectra acquired at 22 °C in a series of $CDCl_3$ solutions with concentrations ranging from 8 μM to 1.7 mM was fit to a dimer model and yielded an association constant of K_a = 66 M^{-1} at 22 °C in $CDCl_3$ (Fig. S27 and S28†). This value suggests C6FE self-associates, but not as strongly as other conjugated structures such as C4BFI (K_a = 725 M^{-1} in $CDCl_3$ at 25 °C) or hexa-*peri*-hexabenzocoronenes with dodecyl chains (K_a = 898 M^{-1} in 1,1,2,2-tetrachloroethane-d_2 at 30 °C).[9,60] We hypothesize that *hex*-C6FE produces a lower association constant than C4FBI due to the larger density of side chains and weaker electron withdrawing ester groups as compared to the diimide groups.

Solid-state organization and Raman spectroscopy

Transesterification was used to exchange the hexyl group for an isopropyl group (Fig. 3b) to evaluate the impact of side chain on solid-state organization. X-ray diffraction patterns of both *hex*-C6FE and *ipr*-C6FE were acquired for powders prepared by precipitation from highly concentrated $CHCl_3$ solutions into methanol (Fig. 3c). Both patterns revealed the samples were partially crystalline with two key sets of Bragg peaks: (i) low q features with spacings corresponding to the overall diameter of macrocycles (25.17 Å for *hex*-C6FE and 20.20 Å for *ipr*-C6FE), and (ii) high q features attributed to π-stacking distances (3.37 Å for *hex*-C6FE and 3.35 Å for *ipr*-C6FE). The higher number of additional distinct reflections in the pattern of *ipr*-C6FE is suggestive of a higher degree of ordering in comparison with *hex*-C6FE.

The higher order of *ipr*-C6FE was also evident in the micro-Raman studies of thin films prepared by drop-casting from $CHCl_3$ (Fig. 3d and e). *Ipr*-C6FE formed small, elongated microcrystals while *hex*-C6FE organized into spherulites reminiscent of those typically observed in partially crystalline polymers. The dominant feature in the Raman spectra was a peak at 1578 cm^{-1}, which corresponds to the symmetric C–C/C=C stretching ("ya" mode),[47] as well as several smaller peaks from 900–1400 cm^{-1}. Interestingly, the intensity of the Raman spectrum for *ipr*-C6FE differed depending on collection location and crystallite orientation relative to the substrate, indicating a high degree of anisotropy within crystallites. In contrast, the Raman spectrum of *hex*-C6FE was minimally dependent on sample location. Analysis of *ipr*-C6FE by IR revealed C=C stretches at 1545 cm^{-1} and 1593 cm^{-1}, as well as a prominent carbonyl stretch at 1713 cm^{-1} from the ester side-chains, and both the Raman and IR spectra are in good agreement with the DFT predicted spectra (Fig. 3e, red plots).

Given that both *ipr*-C6FE and *hex*-C6FE readily formed partially crystalline structures, considerable efforts were made to produce diffraction quality single crystals using a variety of methods such as slow evaporation, slow cooling and vapor diffusion. In contrast with numerous previous studies with other macrocycles of similar size,[9,21,22] none of these efforts yielded crystals of quality sufficient for full structure determination. We hypothesize that this may be related to the asymmetry of the structure, with two possible "heads-to-tails" and "heads-to-heads" (as in stacked coins) arrangements of neighbouring cycles. If neither packing pattern is favoured, mixing of the two packing arrangements may make it difficult to produce single crystals.

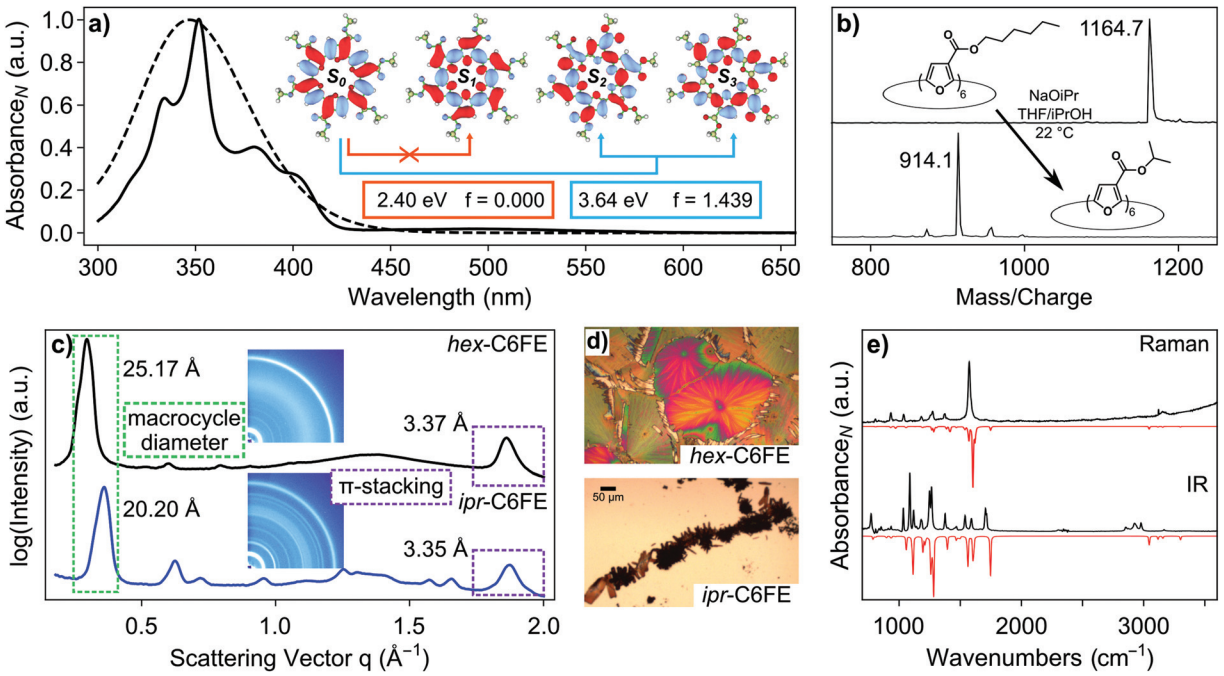

Fig. 3 (a) Normalized absorption spectrum of *hex*-C6FE collected in $CHCl_3$ (solid line) and predicted by TD-DFT (dashed line, CAM-B3LYP-D3 6-31G(d,p) IEFPCM($CHCl_3$)). Also displayed are the calculated natural transition orbitals; the oscillator strength (f) for the $S_0 \rightarrow S_1$ transition (2.43 eV) is 0, and 1.73 for the degenerate $S_0 \rightarrow S_2$ and $S_0 \rightarrow S_3$ transitions (3.57 eV). (b) MALDI-TOF spectra before and after transesterification of *hex*-C6FE to *ipr*-C6FE. (c) Powder X-ray diffraction patterns for *hex*-C6FE (top) and *ipr*-C6FE (bottom). (d) Optical microscope images of *hex*-C6FE (top) and *ipr*-C6FE (bottom) illustrating the difference in solid-state organization upon drop-casting from $CHCl_3$. (e) Experimental (black) and DFT predicted (red, B3LYP-D3 6-31G(d,p)) Raman and IR spectra for *ipr*-C6FE.

Cyclic voltammetry (CV)

CV scans of *hex*-C6FE acquired in CH_2Cl_2 *versus* the saturated calomel reference electrode (SCE) revealed a reversible oxidation at 1.03 V (E_{pa}) and two quasi-reversible oxidations at 1.34 V and 1.52 V (Fig. 4). The first oxidation potential is similar to values reported for oxidation of C4BFI and cyclo[6]pyrrole (~1.25 V and 0.95 V *vs.* SCE, respectively).[9,21] Notably, the first oxidation potential of *hex*-C6FE is higher than a non-cyclic, partially alkylated sexifuran (E_{pa} ~ 0.6 V),[44] reflecting the electron withdrawing nature of ester side groups. This higher resistance to oxidation is also evident in the difference of HOMO energies of these respective species as predicted by DFT (Table S1†).

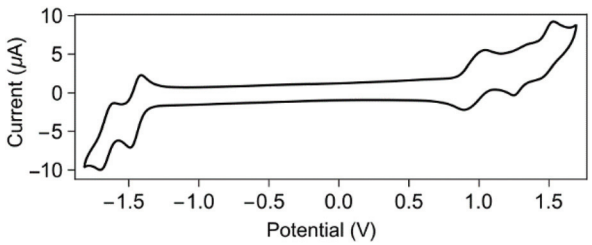

Fig. 4 CV of *hex*-C6FE in degassed CH_2Cl_2 (5 mg mL^{-1}) using NBu_4PF_6 as the supporting electrolyte (0.1 M), with a scan rate of 35 mV s^{-1}. The voltammogram was referenced *versus* SCE using Fc/Fc^+ as an internal standard (0.46 V *vs.* SCE). Determination of the electrochemical band gap of *hex*-C6FE from the onsets of oxidation and reduction at +0.85 and −1.38 V respectively, yielded a value of E_g = 2.23 eV.

Remarkably, *hex*-C6FE produced two reversible reductions at −1.49 V (E_{pc}) and −1.70 V (E_{pc}), and showed no signs of instability after multiple reduction cycles (Fig. S7†). These values are cathodically shifted in comparison with C4BFI and cyclo[6]pyrrole (~−1.0 V and −0.48 V *vs.* SCE, respectively).

There are only a few reports exploring electrochemical reduction of furan oligomers, which may be related to the experimental challenge stemming from their high LUMO levels.[37,44,61,62] The highly reversible electrochemical reduction of C6FE can be partially attributed to the lowering of the LUMO by the ester side groups (−2.61 eV, Table S1†). It is also remarkable since the closely related C4BFI analogue and the helical P3HEF undergo only irreversible reductions, despite the presence of electron-withdrawing side groups.[9,10] The natural question to be raised in discussing the redox properties of cyclic conjugated molecules is the possible role of aromaticity, which is often invoked in such cases. The extent to which this may apply to C6FE is addressed in the next section.

Computed aromaticity of C6FE

Conjugated macrocycles are known to switch between aromatic and antiaromatic states upon successive reductions/oxidations, usually in accordance with Hückel's 4n + 2 rule, as shown previously for cyclo-*para*-phenylenes, for example.[12] The enhanced

electron delocalization from aromatic pathways through the cycle may then render reduced/oxidized states more stable. The potential connection between this effect and C6FE's redox properties was assessed by using DFT results to compute two common aromaticity descriptors: the Nucleus Independent Chemical Shift (NICS)[63] and the Electron Localization Function (ELF)[64,65] (Fig. 5 and 6). In both instances, the calculations revealed globally aromatic character of the dianion and dication, in stark contrast with antiaromatic character of the neutral form.

In NICS calculations, aromaticity is manifested by highly negative values of chemical shift inside of the ring, which are indicative of enhanced diatropic current through the ring, creating a local magnetic magnetic field opposing the external magnetic field. The computed values of the *zz* components of NICS at 1 Å above the plane of C6FE indicate paratropic ring current in the neutral form, corresponding to a formally antiaromatic structure (Fig. 5a). In contrast, the dication and dianion both have negative NICS values inside of the macrocycle and are formally aromatic. These NICS results are consistent with the dominant resonance structures shown for the neutral and charged forms in Fig. 5b. For neutral C6FE, the 24π electrons from the C=C bonds form the dominant resonance pathway (blue bonds in Fig. 5b). This corresponds to 4n π electrons, which is Hückel antiaromatic. Upon $2e^-$ oxidation or reduction, the number of π electrons in the ring system is 4n ± 2, and thus delocalization through these cyclic pathways becomes Hückel aromatic. These proposed aromaticity pathways are also consistent with the picture that emerges from Natural Resonance Theory (NRT)[66–69] analysis (Fig. S26†). More specifically, NRT indicates that the dominant resonance structures, which contribute 83% to the overall electronic structure of the [C6FE],[2] have one negative charge within the furan ring and one on the carbonyl oxygen of the ester side chain.

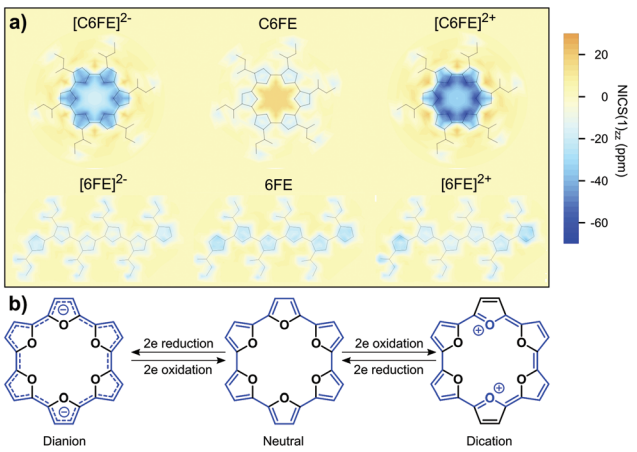

Fig. 5 (a) NICS(1)$_{zz}$ plots for the cyclic (C6FE) and linear (6FE) ester-functionalized furan hexamer. The dianion (left), neutral (middle), and dication (right) are shown. The color scale bar is shown where a more negative value corresponds to a higher degree of aromaticity in the encompassing ring (single furan or entire macrocycle), while a positive number corresponds to a higher degree of antiaromatic character. (b) Annulene-type resonance pathways highlighted by the blue bonds for a six-membered furan macrocycle in the −2 (left), neutral (middle), and +2 states (right).

Similar insights into the electron delocalization pathways in different states of C6FE were obtained by the analysis of the isosurfaces of the ELF, which is defined by $ELF(r) = (1 + (D(r))/D_0(r)^2)^{-1}$. Both $D(r)$ and $D_0(r)$ are computed from the total electron density and correspond, respectively, to the kinetic energy density due to Pauli repulsion and to the Thomas–Fermi kinetic energy density.[65,70] In order to selectively visualize the delocalization of π electrons, the calculations were carried out (using the Multiwfn wavefunction analysis package[71,72]) on combined electron densities from π-orbitals, which were identified by the presence of the node in the plane of the macrocycle. The isosurface value which results in bifurcation of these orbitals along the ring pathway in question serves as a direct indicator of aromaticity. An ELF_π value of 1 indicates perfect delocalization along the path, and benzene serves as a reference point with an ELF_π = 0.91 for all bonds.[64,65] Exploration of other polycylic aromatics suggests an ELF_π = 0.7 as a threshold for aromaticity.[64,65]

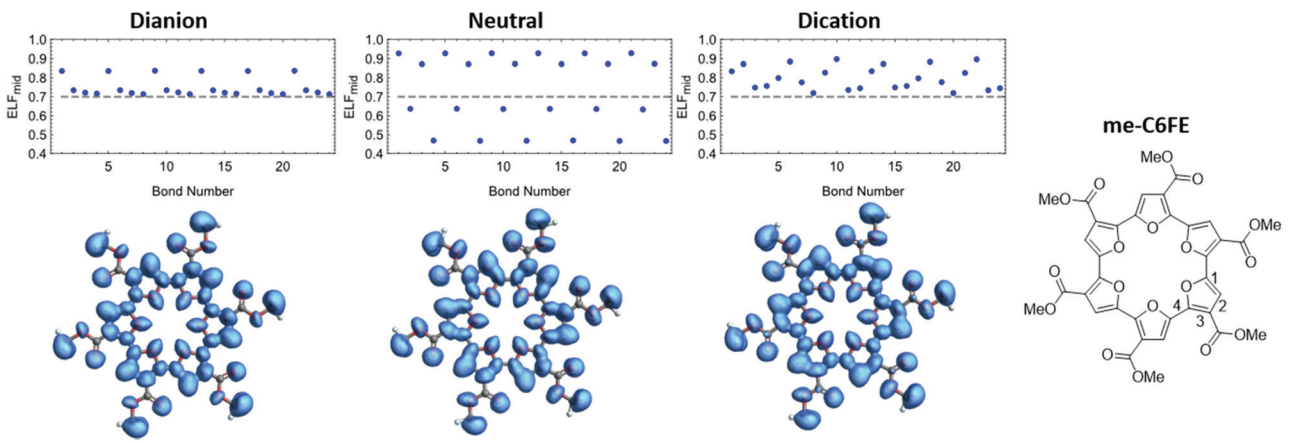

Fig. 6 ELF plots for the *me*-C6FE dianion (left), neutral (middle) and dication (right) plotted with isosurface values of 0.7. Bonds 1 through 4 are labelled and the numbers continue around the macrocycle (24 total bonds). Interring bonds are 4, 8, 12, 16, 20, 24.

For C6FE, the ELF_π value for the interring bond between furan heterocycles is critical to determine effective delocalization across the entire macrocycle (bonds numbered as multiples of 4 in Fig. 6). The ELF_π value of 0.48 for the interring bond in the neutral state is indicative of limited delocalization between heterocycles, while the dication and dianion have ELF_π values of 0.72 for the interring bond, consistent with aromatic character across the entire macrocycle. Overall, these computational results suggest that, in combination with the electron-withdrawing ester side chains, global aromaticity may be a key factor underlying the redox behavior of C6FE.

Conclusions

In conclusion, we have reported the synthesis, characterization, and computational investigation of a novel oligofuran macrocycle (C6FE). A dialkylbiaryl phosphine palladium catalyst was used to synthesize C6FE *via* Suzuki–Miyaura coupling, which is facilitated by an energetic preference for *syn* geometry of adjacent ester-functionalized furan repeat units. MALDI-TOF and NMR were used to confirm formation of the macrocycle, and solid-state characterization revealed partial crystallinity that can be modified by varying side chain identity. Finally, quantum chemistry confirmed that aromaticity played a key role in the observed electrochemical stability upon introduction of charge carriers.[11–14]

Looking forward, the synthetic strategy reported here will be used as a platform to access other macrocycles derived from furan with no linkers present between the repeat units. A natural line of inquiry will be to explore how other heterocyclic building blocks can be incorporated for the synthesis of more complex structures. In particular, introducing sequence, both main chain and side chain, will be of interest to better understand how each of these components impact the properties of these systems. Additionally, the observation that C6FE can be oxidized and reduced reversibly sets the stage for deeper exploration into aromaticity as a tool to enhance stability of π-conjugated systems with furan, which is particularly challenging. Clearly, cyclization of large π-systems offers additional stability as bonding patterns and pathways for charge movement become more diverse. Additional linear and circular π-systems with furan will be explored in more detail in the future.

Conflicts of interest

There are no conflicts of interest to declare.

Acknowledgements

K. J. T. N. is grateful to the ARO (W911NF-16-1-0053) for support of this work.

Notes and references

1 M. Ball, B. Zhang, Y. Zhong, B. Fowler, S. Xiao, F. Ng, M. Steigerwald and C. Nuckolls, Conjugated Macrocycles in Organic Electronics, *Acc. Chem. Res.*, 2019, **52**, 1068–1078.
2 M. Iyoda, J. Yamakawa and M. J. Rahman, Conjugated Macrocycles: Concepts and Applications, *Angew. Chem., Int. Ed.*, 2011, **50**, 10522–10553.
3 M. Iyoda and H. Shimizu, Multifunctional π-expanded Oligothiophene Macrocycles, *Chem. Soc. Rev.*, 2015, **44**, 6411–6424.
4 S. Höger, K. Bonrad, A. Mourran, U. Beginn and M. Möller, Synthesis, Aggregation, and Adsorption Phenomena of Shape-Persistent Macrocycles with Extraannular Polyalkyl Substituents, *J. Am. Chem. Soc.*, 2001, **123**, 5651–5659.
5 Y. Zhong, Y. Yang, Y. Shen, W. Xu, Q. Wang, A. L. Connor, X. Zhou, L. He, X. C. Zeng, Z. Shao, Z.-l. Lu and B. Gong, Enforced Tubular Assembly of Electronically Different Hexakis(*m*-Phenylene Ethynylene) Macrocycles: Persistent Columnar Stacking Driven by Multiple Hydrogen-Bonding Interactions, *J. Am. Chem. Soc.*, 2017, **139**, 15950–15957.
6 Q. Wang, Y. Zhong, D. P. Miller, X. Lu, Q. Tang, Z.-L. Lu, E. Zurek, R. Liu and B. Gong, Self-Assembly and Molecular Recognition in Water: Tubular Stacking and Guest-Templated Discrete Assembly of Water-Soluble, Shape-Persistent Macrocycles, *J. Am. Chem. Soc.*, 2020, **142**, 2915–2924.
7 Y. Tobe, N. Utsumi, K. Kawabata, A. Nagano, K. Adachi, S. Araki, M. Sonoda, K. Hirose and K. Naemura, *m*-Diethynylbenzene Macrocycles: Syntheses and Self-Association Behavior in Solution, *J. Am. Chem. Soc.*, 2002, **124**, 5350–5364.
8 A. S. Shetty, J. Zhang and J. S. Moore, Aromatic π-Stacking in Solution as Revealed through the Aggregation of Phenylacetylene Macrocycles, *J. Am. Chem. Soc.*, 1996, **118**, 1019–1027.
9 S. V. Mulay, O. Dishi, Y. Fang, M. R. Niazi, L. J. W. Shimon, D. F. Perepichka and O. Gidron, A Macrocyclic Oligofuran: Synthesis, Solid State Structure and Electronic Properties, *Chem. Sci.*, 2019, **10**, 8527–8532.
10 A. J. Varni, A. Fortney, M. A. Baker, J. C. Worch, Y. Qiu, D. Yaron, S. Bernhard, K. J. T. Noonan and T. Kowalewski, Photostable Helical Polyfurans, *J. Am. Chem. Soc.*, 2019, **141**, 8858–8867.
11 M. D. Peeks, T. D. W. Claridge and H. L. Anderson, Aromatic and Antiaromatic Ring Currents in a Molecular Nanoring, *Nature*, 2017, **541**, 200–203.
12 N. Toriumi, A. Muranaka, E. Kayahara, S. Yamago and M. Uchiyama, In-Plane Aromaticity in Cycloparaphenylene Dications: A Magnetic Circular Dichroism and Theoretical Study, *J. Am. Chem. Soc.*, 2015, **137**, 82–85.
13 S. Eder, D.-J. Yoo, W. Nogala, M. Pletzer, A. Santana Bonilla, A. J. P. White, K. E. Jelfs, M. Heeney, J. W. Choi and F. Glöcklhofer, Switching Between Local and Global Aromaticity in a Conjugated Macrocycle for High-

Performance Organic Sodium-Ion Battery Anodes, *Angew. Chem., Int. Ed.*, 2020, **59**, 12958–12964.
14 L. Ren, T. Y. Gopalakrishna, I.-H. Park, Y. Han and J. Wu, Porphyrin/Quinoidal-Bithiophene-Based Macrocycles and Their Dications: Template-Free Synthesis and Global Aromaticity, *Angew. Chem., Int. Ed.*, 2020, **59**, 2230–2234.
15 R. Jasti, J. Bhattacharjee, J. B. Neaton and C. R. Bertozzi, Synthesis, Characterization, and Theory of [9]-, [12]-, and [18]Cycloparaphenylene: Carbon Nanohoop Structures, *J. Am. Chem. Soc.*, 2008, **130**, 17646–17647.
16 K. Tahara and Y. Tobe, Molecular Loops and Belts, *Chem. Rev.*, 2006, **106**, 5274–5290.
17 S. E. Lewis, Cycloparaphenylenes and Related Nanohoops, *Chem. Soc. Rev.*, 2015, **44**, 2221–2304.
18 S. Saito and A. Osuka, Expanded Porphyrins: Intriguing Structures, Electronic Properties, and Reactivities, *Angew. Chem., Int. Ed.*, 2011, **50**, 4342–4373.
19 T. Sarma and P. K. Panda, Annulated Isomeric, Expanded, and Contracted Porphyrins, *Chem. Rev.*, 2017, **117**, 2785–2838.
20 M. Buda, A. Iordache, C. Bucher, J.-C. Moutet, G. Royal, E. Saint-Aman and J. L. Sessler, Electrochemical Syntheses of Cyclo[n]pyrrole, *Chem. – Eur. J.*, 2010, **16**, 6810–6819.
21 T. Köhler, D. Seidel, V. Lynch, F. O. Arp, Z. Ou, K. M. Kadish and J. L. Sessler, Formation and Properties of Cyclo[6]pyrrole and Cyclo[7]pyrrole, *J. Am. Chem. Soc.*, 2003, **125**, 6872–6873.
22 D. Seidel, V. Lynch and J. L. Sessler, Cyclo[8]pyrrole: A Simple-to-Make Expanded Porphyrin with No Meso Bridges, *Angew. Chem., Int. Ed.*, 2002, **41**, 1422–1425.
23 P. J. Melfi, S. K. Kim, J. T. Lee, F. Bolze, D. Seidel, V. M. Lynch, J. M. Veauthier, A. J. Gaunt, M. P. Neu, Z. Ou, K. M. Kadish, S. Fukuzumi, K. Ohkubo and J. L. Sessler, Redox Behavior of Cyclo[6]pyrrole in the Formation of a Uranyl Complex, *Inorg. Chem.*, 2007, **46**, 5143–5145.
24 J. T. Lee, D.-H. Chae, Z. Ou, K. M. Kadish, Z. Yao and J. L. Sessler, Unconventional Kondo Effect in Redox Active Single Organic Macrocyclic Transistors, *J. Am. Chem. Soc.*, 2011, **133**, 19547–19552.
25 A. Gorski, T. Köhler, D. Seidel, J. T. Lee, G. Orzanowska, J. L. Sessler and J. Waluk, Electronic Structure, Spectra, and Magnetic Circular Dichroism of Cyclohexa-, Cycloheptа-, and Cyclooctapyrrole, *Chem. – Eur. J.*, 2005, **11**, 4179–4184.
26 J. Krömer, I. Rios-Carreras, G. Fuhrmann, C. Musch, M. Wunderlin, T. Debaerdemaeker, E. Mena-Osteritz and P. Bäuerle, Synthesis of the First Fully α-Conjugated Macrocyclic Oligothiophenes: Cyclo[n]thiophenes with Tunable Cavities in the Nanometer Regime, *Angew. Chem., Int. Ed.*, 2000, **39**, 3481–3486.
27 F. Zhang, G. Götz, H. D. F. Winkler, C. A. Schalley and P. Bäuerle, Giant Cyclo[n]thiophenes with Extended π Conjugation, *Angew. Chem., Int. Ed.*, 2009, **48**, 6632–6635.
28 F. Zhang, G. Götz, E. Mena-Osteritz, M. Weil, B. Sarkar, W. Kaim and P. Bäuerle, Molecular and Electronic Structure of Cyclo[10]thiophene in Various Oxidation States: Polaron Pair vs. Bipolaron, *Chem. Sci.*, 2011, **2**, 781–784.
29 F. Sannicolò, P. R. Mussini, T. Benincori, R. Cirilli, S. Abbate, S. Arnaboldi, S. Casolo, E. Castiglioni, G. Longhi, R. Martinazzo, M. Panigati, M. Pappini, E. Quartapelle Procopio and S. Rizzo, Inherently Chiral Macrocyclic Oligothiophenes: Easily Accessible Electrosensitive Cavities with Outstanding Enantioselection Performances, *Chem. – Eur. J.*, 2014, **20**, 15298–15302.
30 K. Asai, A. Fukazawa and S. Yamaguchi, A Cyclic Octithiophene Containing β,β′-Linkages, *Chem. Commun.*, 2015, **51**, 6096–6099.
31 E. Quartapelle Procopio, T. Benincori, G. Appoloni, P. R. Mussini, S. Arnaboldi, C. Carbonera, R. Cirilli, A. Cominetti, L. Longo, R. Martinazzo, M. Panigati and R. Pò, A Family of Solution-Processable Macrocyclic and Open-Chain Oligothiophenes with Atropoisomeric Scaffolds: Structural and Electronic Features for Potential Energy Applications, *New J. Chem.*, 2017, **41**, 10009–10019.
32 K. Kise, F. Chen, K. Kato, T. Tanaka and A. Osuka, Cyclic Hybrids of Alternately Linked 2,5-Pyrrolylenes and 3,4-Thienylenes, *Chem. Lett.*, 2017, **46**, 1319–1322.
33 T. Iwanaga, Y. Yamada, T. Yamauchi, Y. Misaki, M. Inoue and H. Yamada, A Saddle-shaped Macrocycle Comprising 2,5-Diphenylthiophene Units, *Chem. Lett.*, 2018, **47**, 760–762.
34 G. Fuhrmann, T. Debaerdemaeker and P. Bäuerle, C–C Bond Formation Through Oxidatively Induced Elimination of Platinum Complexes—A Novel Approach Towards Conjugated Macrocycles, *Chem. Commun.*, 2003, 948–949, DOI: 10.1039/B300542A.
35 K. J. Weiland, T. Brandl, K. Atz, A. Prescimone, D. Häussinger, T. Šolomek and M. Mayor, Mechanical Stabilization of Helical Chirality in a Macrocyclic Oligothiophene, *J. Am. Chem. Soc.*, 2019, **141**, 2104–2110.
36 S. S. Zade and M. Bendikov, Twisting of Conjugated Oligomers and Polymers: Case Study of Oligo- and Polythiophene, *Chem. – Eur. J.*, 2007, **13**, 3688–3700.
37 O. Gidron, Y. Diskin-Posner and M. Bendikov, α-Oligofurans, *J. Am. Chem. Soc.*, 2010, **132**, 2148–2150.
38 O. Gidron, A. Dadvand, Y. Sheynin, M. Bendikov and D. F. Perepichka, Towards "Green" Electronic Materials. α-Oligofurans as Semiconductors, *Chem. Commun.*, 2011, **47**, 1976–1978.
39 O. Gidron, A. Dadvand, E. Wei-Hsin Sun, I. Chung, L. J. W. Shimon, M. Bendikov and D. F. Perepichka, Oligofuran-Containing Molecules for Organic Electronics, *J. Mater. Chem. C*, 2013, **1**, 4358–4367.
40 O. Gidron, Y. Diskin-Posner and M. Bendikov, High Charge Delocalization and Conjugation in Oligofuran Molecular Wires, *Chem. – Eur. J.*, 2013, **19**, 13140–13150.
41 O. Gidron, N. Varsano, L. J. W. Shimon, G. Leitus and M. Bendikov, Study of a Bifuran vs. Bithiophene Unit for the Rational Design of π-Conjugated Systems. What Have We Learned?, *Chem. Commun.*, 2013, **49**, 6256–6258.

42 S. Sharma and M. Bendikov, α-Oligofurans: A Computational Study, *Chem. – Eur. J.*, 2013, **19**, 13127–13139.
43 O. Gidron and M. Bendikov, α-Oligofurans: An Emerging Class of Conjugated Oligomers for Organic Electronics, *Angew. Chem., Int. Ed.*, 2014, **53**, 2546–2555.
44 X.-H. Jin, D. Sheberla, L. J. W. Shimon and M. Bendikov, Highly Coplanar Very Long Oligo(alkylfuran)s: A Conjugated System with Specific Head-To-Head Defect, *J. Am. Chem. Soc.*, 2014, **136**, 2592–2601.
45 S. Sharma, N. Zamoshchik and M. Bendikov, Polyfurans: A Computational Study, *Isr. J. Chem.*, 2014, **54**, 712–722.
46 D. Sheberla, S. Patra, Y. H. Wijsboom, S. Sharma, Y. Sheynin, A.-E. Haj-Yahia, A. H. Barak, O. Gidron and M. Bendikov, Conducting Polyfurans by Electropolymerization of Oligofurans, *Chem. Sci.*, 2015, **6**, 360–371.
47 O. Dishi and O. Gidron, Macrocyclic Oligofurans: A Computational Study, *J. Org. Chem.*, 2018, **83**, 3119–3125.
48 W. Haas, B. Knipp, M. Sicken, J. Lex and E. Vogel, Tetraoxaporphyrinogen (Tetraoxaquaterene) - Oxidation to the Tetraoxaporphyrin Dication, *Angew. Chem., Int. Ed.*, 1988, **27**, 409–411.
49 E. Vogel, W. Haas, B. Knipp, J. Lex and H. Schmickler, Tetraoxaporphyrin Dication, *Angew. Chem., Int. Ed.*, 1988, **27**, 406–409.
50 E. Vogel, M. Sicken, P. Rohrig, H. Schmickler, J. Lex and O. Ermer, Tetraoxaporphycene Dication, *Angew. Chem., Int. Ed.*, 1988, **27**, 411–414.
51 M. Pohl, H. Schmickler, J. Lex and E. Vogel, Isophlorins - Molecules at the Crossroads of Porphyrin and Annulene Chemistry, *Angew. Chem., Int. Ed.*, 1991, **30**, 1693–1697.
52 E. Vogel, The Porphyrins from the Annulene Chemists Perspective, *Pure Appl. Chem.*, 1993, **65**, 143–152.
53 N. C. Bruno, M. T. Tudge and S. L. Buchwald, Design and Preparation of New Palladium Precatalysts for C–C and C–N Cross-Coupling Reactions, *Chem. Sci.*, 2013, **4**, 916–920.
54 E. E. Sheina, J. Liu, M. C. Iovu, D. W. Laird and R. D. McCullough, Chain Growth Mechanism for Regioregular Nickel-Initiated Cross-Coupling Polymerizations, *Macromolecules*, 2004, **37**, 3526–3528.
55 P. Kohn, S. Huettner, H. Komber, V. Senkovskyy, R. Tkachov, A. Kiriy, R. H. Friend, U. Steiner, W. T. S. Huck, J. U. Sommer and M. Sommer, On the Role of Single Regiodefects and Polydispersity in Regioregular Poly(3-hexylthiophene): Defect Distribution, Synthesis of Defect-Free Chains, and a Simple Model for the Determination of Crystallinity, *J. Am. Chem. Soc.*, 2012, **134**, 4790–4805.
56 V. Martí-Centelles, M. D. Pandey, M. I. Burguete and S. V. Luis, Macrocyclization Reactions: The Importance of Conformational, Configurational, and Template-Induced Preorganization, *Chem. Rev.*, 2015, **115**, 8736–8834.
57 R. B. Martin, Comparisons of Indefinite Self-Association Models, *Chem. Rev.*, 1996, **96**, 3043–3064.
58 M. Chu, A. N. Scioneaux and C. S. Hartley, Solution-Phase Dimerization of an Oblong Shape-Persistent Macrocycle, *J. Org. Chem.*, 2014, **79**, 9009–9017.
59 P. T. Lynett and K. E. Maly, Synthesis of Substituted Trinaphthylenes via Aryne Cyclotrimerization, *Org. Lett.*, 2009, **11**, 3726–3729.
60 M. Kastler, W. Pisula, D. Wasserfallen, T. Pakula and K. Müllen, Influence of Alkyl Substituents on the Solution- and Surface-Organization of Hexa-peri-hexabenzocoronenes, *J. Am. Chem. Soc.*, 2005, **127**, 4286–4296.
61 S. Glenis, M. Benz, E. LeGoff, J. L. Schindler, C. R. Kannewurf and M. G. Kanatzidis, Polyfuran: A New Synthetic Approach and Electronic Properties, *J. Am. Chem. Soc.*, 1993, **115**, 12519–12525.
62 J. K. Politis, J. C. Nemes and M. D. Curtis, Synthesis and Characterization of Regiorandom and Regioregular Poly(3-octylfuran), *J. Am. Chem. Soc.*, 2001, **123**, 2537–2547.
63 Z. Chen, C. S. Wannere, C. Corminboeuf, R. Puchta and P. v. R. Schleyer, Nucleus-Independent Chemical Shifts (NICS) as an Aromaticity Criterion, *Chem. Rev.*, 2005, **105**, 3842–3888.
64 J. Poater, M. Duran, M. Solà and B. Silvi, Theoretical Evaluation of Electron Delocalization in Aromatic Molecules by Means of Atoms in Molecules (AIM) and Electron Localization Function (ELF) Topological Approaches, *Chem. Rev.*, 2005, **105**, 3911–3947.
65 J. C. Santos, W. Tiznado, R. Contreras and P. Fuentealba, Sigma–pi Separation of the Electron Localization Function and Aromaticity, *J. Chem. Phys.*, 2004, **120**, 1670–1673.
66 E. D. Glendening, C. R. Landis and F. Weinhold, Resonance Theory Reboot, *J. Am. Chem. Soc.*, 2019, **141**, 4156–4166.
67 E. D. Glendening, J. K. Badenhoop and F. Weinhold, Natural Resonance Theory: III. Chemical Applications, *J. Comput. Chem.*, 1998, **19**, 628–646.
68 E. D. Glendening and F. Weinhold, Natural Resonance Theory: I. General Formalism, *J. Comput. Chem.*, 1998, **19**, 593–609.
69 E. D. Glendening and F. Weinhold, Natural Resonance Theory: II. Natural Bond Order and Valency, *J. Comput. Chem.*, 1998, **19**, 610–627.
70 J. C. Santos, J. Andres, A. Aizman and P. Fuentealba, An Aromaticity Scale Based on the Topological Analysis of the Electron Localization Function Including σ and π Contributions, *J. Chem. Theory Comput.*, 2005, **1**, 83–86.
71 T. Lu and F. Chen, Multiwfn: A multifunctional wavefunction analyzer, *J. Comput. Chem.*, 2012, **33**, 580–592.
72 T. Lu and F. Chen, Meaning and Functional Form of the Electron Localization Function, *Acta Phys.–Chim. Sin.*, 2011, **27**, 2786–2792.

